



Physical Chemistry Chemical Physics



Accepted Manuscript

This article can be cited before page numbers have been issued, to do this please use: N. V. Karimova, O. Alija, S. L. Mora Garcia, V. Grassian, R. B. Gerber and J. Navea, *Phys. Chem. Chem. Phys.*, 2023, DOI: 10.1039/D3CP01520C.



This is an Accepted Manuscript, which has been through the Royal Society of Chemistry peer review process and has been accepted for publication.

Accepted Manuscripts are published online shortly after acceptance, before technical editing, formatting and proof reading. Using this free service, authors can make their results available to the community, in citable form, before we publish the edited article. We will replace this Accepted Manuscript with the edited and formatted Advance Article as soon as it is available.

You can find more information about Accepted Manuscripts in the <u>Information for Authors</u>.

Please note that technical editing may introduce minor changes to the text and/or graphics, which may alter content. The journal's standard <u>Terms & Conditions</u> and the <u>Ethical guidelines</u> still apply. In no event shall the Royal Society of Chemistry be held responsible for any errors or omissions in this Accepted Manuscript or any consequences arising from the use of any information it contains.



pH Dependence of the Speciation and Optical Properties of 4-Benzoylbenzoic Acid

Natalia Karimova¹, Onita Alija², Stephanie L. Mora García³, Vicki H. Grassian³, R. Benny Gerber^{1,4}, and Juan G. Navea^{2,*}

¹Department of Chemistry, University of California Irvine, CA 92697, USA
 ²Chemistry Department, Skidmore College, Saratoga Springs, NY, 12866-1632, USA
 ³Department of Chemistry, University of California San Diego, CA 92093, USA
 ⁴The Institute of Chemistry and Fritz Haber Research Center, The Hebrew University of Jerusalem, 91904 Jerusalem, Israel

* Corresponding author: Juan G. Navea, jnavea@skidmore.edu

Abstract

Organic chromophores initiate much of daytime aqueous phase chemistry in the environment. Thus, studying the absorption spectra of commonly used organic photosensitizers is paramount to fully understand their relevance in environmental processes. In this work, we combined UV-Vis spectroscopy, ¹H-NMR spectroscopy, quantum chemical calculations, and molecular dynamics to investigate the absorption spectra of 4-benzovl benzoic acid (4BBA), a widely used photosensitizer and common proxy of environmentally relevant chromophores. Solutions of 4BBA at different pH show that protonated and deprotonated species have an effect in its absorbance spectra. Theoretical calculations of these species in water clusters provide physical and chemical insight into the spectra. Quantum chemical calculations were conducted to analyze the UV-Vis absorbance spectra of 4BBA species using various cluster sizes, such as (C₆H₅COC₆H₄COOH·(H₂O)_n) where n = 8 for a relatively small clusters or n=30 for larger clusters. While relatively small clusters have successfully been used for smaller chromophores, our results indicate that simulations of protonated species of 4BBA require relatively larger clusters of n=30. A comparison between experimental and theoretical results shows good agreement in the pH-dependent spectral shift between the hydrated cluster model and the experimental data. Overall, theoretical and empirical results indicate that the experimental optical spectra of aqueous phase 4BBA can be represented by the acid-base equilibrium of the keto-forms, with a spectroscopically measured pKa of $3.41 \pm$ 0.04. Results summarized here contribute to a molecular-level understanding of solvated organic molecules through calculations restricted to clusters models, and thereby, broader insight into environmentally relevant chromophores.

Introduction

Light-absorbing organic acids are ubiquitous chromophores in natural systems and play a significant role in the daytime chemistry of the environment.¹⁻⁷ These organic acids are important fractions of dissolved organic matter (DOM), one of the most abundant and strongest light-absorbing compounds in environmental aqueous systems.⁸⁻¹⁴ The fraction of DOM that absorbs ultraviolet (UV) and visible light is referred as chromophoric dissolved organic matter (CDOM), commonly found in the sea surface microlayer and, more recently, within sea spray aerosol.¹⁴⁻¹⁸ These chromophores are effective photosensitizers,^{19,20} exhibiting strong absorption bands that extend into the visible spectral region, overlapping with the solar spectral flux.^{3,21-30} Given that naturally occurring photosensitizers are known to induce photochemical reactions in aqueous environments, both in bulk and interface, the understanding of these photochemical processes are significant from an atmospheric point of view.³¹⁻³³ In particular, studies that combine experimental techniques with theoretical simulations have provided deeper insight into the processes of photoactivation of molecules at interfaces.^{1,34-36}

Present knowledge on this topic is incomplete due to the complex composition of CDOM. A recent analysis by Alves et al. shows that CDOM is rich in aromatic ketones, aldehydes, carboxyl alicyclic molecules, among other classes of compounds.³⁷ Theoretical and experimental investigations of small molecules matching these molecular moieties can provide insights into the optical properties of these more complex light absorbing substances and the role of environmental factors (pH, hydration state etc.) in these properties.^{1,36,38,39} For instance, studies of the optical properties of simple isolated molecules, such as benzoic¹ and pyruvic acids,³⁶ have been shown to mimic some of the photochemistry and photophysics properties of CDOM in a simple-to-complex approach, leading to a possible molecular structure of CDOM presented through a large realistic

simulation, where aromaticity is shown to play a significant role.³⁴ 4-benzoylbenzoic acid (4BBA), a well-known photosensitizer, has been used as a model to mimic the optical properties of more complex marine CDOM.^{5,40-43} Aromatic carboxylic acids have strong absorption bands in the UV spectral region above 290 nm, overlapping with the solar spectral region.^{44,45} With a relatively low solubility, 4BBA can be considered as one possible model of marine CDOM and terrestrial humic substances that mimic the aromatic fraction of the chromophores. Yet, little is known about the optical properties and excited states of this widely used photosensitizer, especially in the context of environmental factors such as pH.

For example, the photoactivity of 4BBA, like those of other carboxylic acids and chromophores in CDOM, can change with pH.^{1,36} Protonation and deprotonation of keto organic acids such as 4BBA, a common moiety within CDOM, can establish a hydrate under acidic conditions, leading to a possible keto-diol equilibrium, as shown in Scheme 1. These possible increase in keto-acids speciation has the potential to impact the optical properties and photoactivation of photosensitizers.³⁶ This is particularly important considering the wide pH variations in the marine atmosphere, with a basic sea surface microlayer (SSML) of pH \approx 8, and nascent sea spray aerosol (nSSA) reaching acidic conditions of pH \approx 2,⁴⁶ a more typical pH for aerosol deliquescent layer.^{3,47-51}

Scheme 1. Possible equilibria of species found in aqueous solutions of keto acids. R represents an organic group, with [R] including the possible absence of it.

Thus, any keto acid molecular model system needs to consider the more complex speciation arising from hydrate equilibria. Acidification of aqueous phase molecular models, such as 4BBA, impacts the photophysics and photochemistry by shifting the speciated forms of the organic molecule from neutral to protonated forms. 36,52 It is, thus, paramount to investigate the pH-induced changes in photoactivity of molecular models of environmental photosensitizers to better understand their role in daytime chemistry. Although the 4BBA molecule is a relatively simple system, the possibility of hydration in the keto group, leading to a geminal diol-form of protonated and deprotonated species has not been investigated.

In this work, we carried out experimental spectroscopic measurements combined with theoretical calculations to study the optical properties of 4BBA in aqueous solution at different pHs, providing insight on both the acid form and its conjugate base. We elucidate the speciation of 4BBA as a function of pH and show the effects of protonation in its optical properties. Titrations of 100 μ M 4BBA solutions were carried out from pH = 1.0 to pH = 12.0, with UV-Vis spectral data collected at each pH unit in order to determine the pKa of the system. A major challenge of the current study is the complexity of the photophysical and photochemical properties of 4BBA in solution. These challenges arise from: (i) medium effects –solvent molecules have been shown to

have an effect in the structure of chromophoric compounds in environmental interfaces; 1,36 (ii) the contribution of the different speciated forms to the optical absorption spectrum have not been investigated and; (iii) 4BBA, the molecule of interest here, is a relatively large molecule compared to what has been done in previous studies. Along with aromaticity, larger molecular species make the calculations computationally challenging, especially when solvent molecules are included (the largest system contains around 120 atoms). Here, our calculations provide insight on: (i) the nature of 4BBA excited states; (ii) solvent effects; (iii) orbitals participated in the electron transition, and (iv) the contribution of speciated forms to the 4BBA optical spectrum at different pH.

Experimental methods and materials.

Optical properties and speciation analysis

The chromophore 4-benzovl benzoic acid (4BBA) was purchased from Sigma Aldrich and used without further purification. Aqueous solutions of 4BBA were prepared using 18 M Ω Milli-Q water at concentrations of 100 µM. All the pH adjustments were carried out by adding either hydrochloric acid (1 N stock solution) or sodium hydroxide (1 N stock solution), both solutions from Fisher Chemical. Potentiometric titration for the measurement of pKa and pH measurements were carried out using an ACUMET AB15 pH meter. All UV-Vis spectral data was acquired using a Perkin Elmer Lambda 35 spectrophotometer. Speciation and further pK_a studies were carried out by ¹H-NMR performed using a 500 Jeol ECA NMR spectrometer with solvent suppression in the acquisition parameters. The solutions contained 10% D₂O for instrument locking and 5uM sodium trimethylsilylpropanesulfonate (DSS) purchased from Sigma Aldrich was used as the internal standard for peak locking.

In order to determine if the observed optical changes correspond to acid-base equilibria of the keto acid for of 4BBA, or a more complex speciation is responsible for the changes in the optical spectra of 4BBA, a combination of potentiometric titration and solvent-suppression ¹H-NMR spectra were carried out. The UV-Vis spectra for the 100 μ M solution of 4BBA at pHs was acquired at pHs ranging from 1.0 to 12.0. Similarly, ¹H-NMR were collected for solutions with pHs from 1.0 to 7.0.

Theoretical Models and Methods

To better understand the water-4BBA interaction as a function of pH, theoretical spectra of all possible forms of 4BBA, as described in **Scheme 1**, were simulated and compared with UV-Vis spectral data of 4BBA. To confirm the NMR spectral data, keto and diol-forms of water-4BBA protonated and deprotonated were also calculated and its absorption spectra simulated. In this work, theoretical results of neutral keto- and diol-forms of 4BBA were associated with the experimental spectrum measured at pH=1, whereas the deprotonated keto- and diol-forms of 4BBA were considered as possible models for the experimental spectrum of 4BBA at pH=6. This pH range around pK_{a,1} is used to model the protonated and deprotonated species, allowing the study of which speciated form of 4BBA is favored at low and high pH.

Small clusters - $4BBA \cdot (H_2O)_8$. Recent works showed that solvent effects play a crucial role in the quality of the simulated spectra of benzoic acid and humic substances. ^{1,34} Without including water molecules in the model system it is almost impossible to reproduce experimental results, especially for experiments at high pH when deprotonated speciated forms are dominant. This indicates that water solvation contributes to the electron excitation of the chromophore. According to previous studies involving benzoic acid, ¹ a total of eight water molecules in addition to the extended solvent

environment (polarizable continuum model) provide a good agreement with the experiment, in particular, the shape and the positions of the peaks. Therefore, as a first step of the present work, clusters of 4BBA species with 8 water molecules were considered - 4BBA (H₂O)₈. The initial water cluster structure and its position near 4BBA, was modeled based on the methods implemented in the theoretical study of benzoic acid. Accordingly, water molecules were only located near the carboxylic acid group and do not interact with keto- and diol-groups of 4BBA (Figure 1).¹

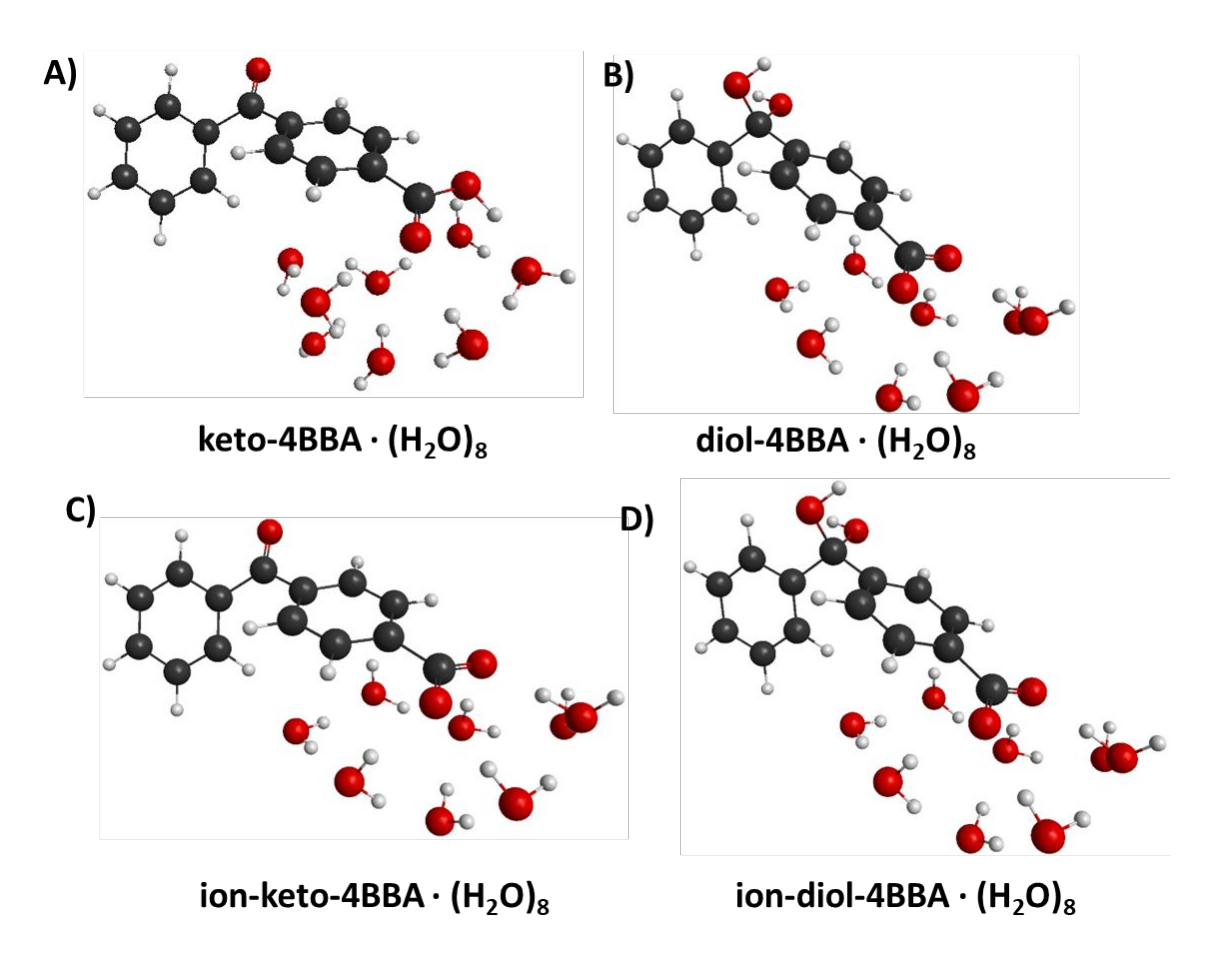


Figure 1. Geometrical structures of hydrated 4BBA molecules: (A) neutral keto-form of 4BBA, (B) neutral diol-form of 4BBA, (C) deprotonated keto-form of 4BBA, and (D) deprotonated diolform of 4BBA.

All theoretical calculations for small clusters 4BBA·(H₂O)₈ were performed using Density Functional Theory (DFT) and Time-Dependent DFT (TD-DFT) methods within the Q-Chem program.⁵³ Geometry optimizations employ the B3LYP functional⁵⁴ and basis set 6-31+G*, with dispersion corrections from Grimme's DFT-D2.55 For calculations of excited states, the explicit solvent molecules (water clusters in our suggested models) were combined with the polarizable continuum model (C-PCM).56 Solute cavities are constructed from a union of atom-centered spheres whose radii are 1.2 times the atomic van der Waals radii suggested by Bondi.⁵⁷ The choice of functional and basis set is crucial in accurately studying molecular systems. Here, B3LYP/6-311++G** method was selected. This functional and basis set combination has been successfully applied before to study the benzoic acid (BA). In this study, the B3LYP functional was assessed with various standard basis sets, including Pople (6-31+G*, 6-311+G*, 6-311++G**) and Dunning (aug-cc-pVTZ and aug-cc-pVQZ) basis sets. The results revealed that the aug-cc-pVTZ and 6-311++G** basis sets provided the closest agreement to the aug-cc-pVQZ basis set, which is known for its accuracy. Therefore, using the Pople's basis set 6-311++G** can be a reasonable alternative that saves computational time compared to the more expensive augmented Dunning's basis sets. This finding suggests that by employing the appropriate basis set, reliable results can be obtained while reducing the computational cost.

To assess the accuracy of the B3LYP functional in predicting the optical absorption spectra of 4BBA systems, we performed a comprehensive comparative analysis involving various functionals such as B3LYP, CAM-B3LYP, LRC-wPBEh, and wB97X. The calculations focused on the neutral keto-form of the 4BBA·(H₂O)₈ complex, and the obtained spectra were compared to the experimental data obtained at pH=1. The findings of this investigation will be discussed in detail in the forthcoming "Results and Discussion" section.

This relatively small size of this water cluster limits the solvent interaction with 4BBA to the carboxyl group, leaving the keto/diol groups with no solvating water interactions. To gain deeper insights into the nature of the excited states responsible for the I- and II-bands, we conducted calculations of hole/particle Natural Transition Orbitals (NTOs) pairs using the B3LYP/6-311++G** method. Additionally, we explored the NTOs for the neutral keto-form of 4BBA·(H₂O)₈ by employing the CAM-B3LYP/6-311++G** method in the gas phase to evaluate if there is the extent of orbital delocalization and investigate the potential contribution of water molecules in the excited states if any. This allowed us to examine if there is the possibility of charge transfer phenomena as the system's cluster size increased, which can be missed due to the B3LYP functional. CAM-B3LYP is known to be superior to B3LYP for studying charge transfer phenomena due to its ability to capture long-range electron transfer interactions accurately. Unlike B3LYP, which treats all electron-electron interactions equally, CAM-B3LYP incorporates a longrange correction that improves the description of charge transfer states. This correction accounts for a fraction of Hartree-Fock exchange that contributes to long-range electron-electron interactions, which are crucial for charge transfer phenomena. The outcomes of these calculations will be extensively discussed, shedding light on the underlying electronic characteristics of the specific excited states under investigation.

Large clusters - $4BBA \cdot (H_2O)_{30}$. To include interactions of solvent media with all functional groups present in the 4BBA molecule (keto-, diol- and carboxy-groups), large water clusters (30 water molecules) were used. Due to the system size of large clusters, the calculation of excited states using traditional *ab initio* approaches are very challenging and computationally expensive. One possible method that can accurately describe structural and optical effects in large systems with a reasonable computational cost is the density functional tight-binding (DFTB) method⁵⁹ and excited states formalism TD-DFTB, ^{59,60} which aims to achieve the accuracy of DFT methods and the

efficiency of tight-binding-based methods. To include all possible speciated forms into the total optical spectrum, the combination of Molecular Dynamics DFTB (MD-DFTB) method with TD-DFTB was used. This approach was previously used for the simulation of β -hydroxyalkyl nitrates, pyruvic acid, benzoic acid, and humic substances.^{1,34,38,61}

For large systems, all calculations were performed using the DFTB+ (18.2 version) package.⁶² Calculations were performed using the DFTB3-D3H5 formalism ^{60,63} and the 3ob-3-1 parameter set. 64-66 DFTB-D3H5 is a variant of DFTB3 with additional corrections for non-covalent interactions, including dispersion and hydrogen bonds. For a DFTB3-D3H5 calculation, a specific parametrization of the dispersion correction (DftD3) has to be used: $sr_6 = 1.25$; alpha₆ = 29.62; s_6 = 1.0; and $s_8 = 0.49$.65 In addition, the hydrogen-hydrogen repulsion was also activated.67 The maximum angular momentum was set to: H = s; C = p; O = p; and N = p. The Hubbard derivatives (in atomic units) were specified for the selected parameter set: H = -0.1857; C = -0.1492; O = -0.14920.1575; and N = -0.1535. Excited states of the molecule 4BBA in a water cluster were calculated using TD-DFTB method⁶² as implemented in the DFTB+ package. To generate initial structures for four distinct forms of 4BBA, the most energetically preferable geometries of 4BBA (obtained in a gas phase using B3LYP/6-31+G* method) were surrounded by 30 water molecules. Packmol⁶⁸ program was used to randomly distribute these 30 water molecules around the 4BBA molecule, specifically placed into a center of the cluster sphere (radius 8 Å). Obtained geometries were optimized by DFTB and then used as an initial structure for MD-DFTB calculations.

All MD calculations were performed at constant energy. Initial velocities were sampled for the equilibrium structure of interest from a Boltzmann distribution at 298 K. The time-step was 0.4 fs, with a total of 40 trajectories, 10 of these trajectories were simulated for 4BBA·(H₂O)₃₀ per isomer. The total calculation time is around 10 ps per trajectory. Each of these trajectories was

used for the calculation of the total optical absorption spectrum: we extracted structures every 250 fs of the simulation, and their vertical excitation energies and oscillator strengths were calculated with TD-DFTB. All the resulting Gaussian were added to yield the excitation spectrum. This approach has been successfully implemented for the simulation of β -hydroxyalkyl nitrates, pyruvic and benzoic acids. 1,38,61

To assess the performance of the TD-DFTB method, we conducted a comparative analysis of the optical absorption spectra obtained using the tight-binding approach and the TD-DFT method. Specifically, we examined the optical spectra of the neutral and ionized keto-forms of the 4BBA·(H₂O)₃₀, which were selected from the DFTB-MD trajectories. Our findings indicate that there is no significant difference in the curve shape of the optical spectra obtained with both methods. In the case of the neutral structure, the maximum difference in peak positions between TD-DFTB and TD-DFT is only 3 nm, as depicted in **Figure S2** of the Supporting Information. However, for the anionic structure, there is a notable redshift of approximately 20 nm in TD-DFTB compared to TD-DFT. Overall, the results demonstrate that TD-DFTB yields reasonable agreement with TD-DFT in reproducing the optical absorption spectra for both the neutral and anionic structures of 4BBA. This suggests that TD-DFTB can be a reliable alternative method for studying the optical properties of these systems.

The optical spectra were simulated by convoluting the vertical transitions at each excitation energy with a Gaussian line shape. The selection of the full width at half-maximum (FWHM) for the Gaussian was based on the experimental FWHM, which ranged between 0.39 and 0.42 eV. To simplify the calculations, the FWHM value was approximated as 0.4 eV. Subsequently, all spectra were convolved in energy units (eV). Then the result was converted to wavelength units (nm) using the formula $\lambda(nm) = 1239.9/E(eV)$, where λ represents the wavelength and E denotes the energy.

Results and Discussion

Experimental results.

The UV-Vis spectra for 100 µM solutions of 4BBA at pHs 1.0 to 12.0 is shown in **Figure 2A**. At low pHs, two bands are clearly observed, highlighted as minima in the first-order derivative of the UV-Vis spectra (**Figure 2B**): an intense I-band centered at 260 nm and a II-band at 333nm. The I-band has a long absorbance tail across all pHs examined, reaching the visible spectral region. Between pHs 1.0 to 3.0, there are no significant changes in the spectral features of the solution. As pH increases from 3.0 to 4.0 a small redshift of 4 nm in the I-band is observed, after which the intensity of the I-band decreases and remains relatively contestant up to pH 12.0. Above pH 4.0, the II-band is no longer observable.

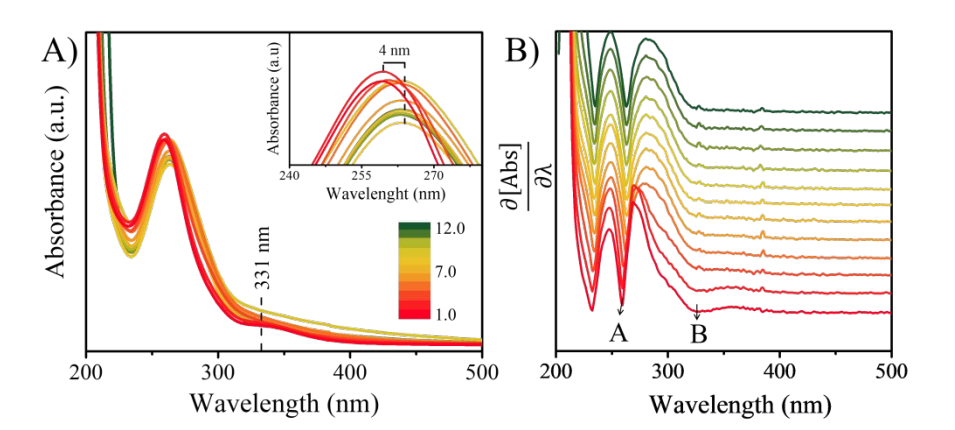


Figure 2. (A) Representative UV–vis absorption spectra of 100 μM 4BBA solutions over a range of pH conditions from 1.0 to 12.0. Insert shows the redshift of band I. (B) First order derivative of spectral data, showing minima for bands I and II.

As shown in Scheme 1, keto acids can be found in protonated and deprotonated forms.⁶⁹ In order to determine whether the diol or keto-forms of 4BBA are present in aqueous phase, a pH-dependent ¹H-NMR analysis was carried out at 22 °C (Support Materials, **Figure 1S**). This keto-diol equilibrium has been observed in other environmentally relevant keto acids. While the diol-form is not stable isolated, its presence in solution is possible and can increase the speciation of

the system. This ¹H-NMR analysis shows no detectable formation of the diol in solution phase at any of the pHs examined. Thus, the speciation of 4BBA is primarily the acid and conjugate base of the keto-form, without any diol species detected:

$$OH \longleftrightarrow O^{-} + H^{+}$$

$$(1)$$

Aromatic rings will tend to make the carbon in the keto group more electrophilic by induction, which would favor hydration and the formation of gem-diol species in aqueous phase.⁶⁹ However, resonance effects make the carbon in the keto group less electrophile, driving the charge density and thus preventing the formation of diols for 4BBA in aqueous solutions.⁶⁹ ¹H-NMR only shows the keto-form of 4BBA, with the expected shifts in the spectra as protonation/deprotonation of the carboxylic acid takes place.

Fitting of the NMR spectral data shifts in response to acid and conjugate base equilibrium yields a pKa of 3.41±0.02 (Supplementary Information, Figure S1B and S1C). Previous 4BBA pKa measurements have place the pKa near 4.85,70 yet these measurements were conducted in 50% ethanol solutions, in order to increase the solubility of 4BBA. In addition to ¹H-NMR, the acid-base equilibrium of 4BBA was investigated in 18 M Ω water via potentiometric titration, resulting in a pKa = 3.41 ± 0.04 (Supplementary Information, Figure S1A), a statistically similar value than that reported via ¹H-NMR analysis. Thus, the UV-Vis absorption spectra below pH 3.0 represent that of neutral 4BBA, with over 98% of species in neutral form. Absorption spectra taken above pH 6 represent that of anionic species as the system is more than 99% deprotonated. At acidic pH, neutral 4BBA shows higher absorbance in the I-band and II-band. As pH increases, forming deprotonated species, the I-band at 260 nm redshifts to 264 nm and the II-band is not observable above pH 4.

The NMR analysis and pH-dependent changes in the optical properties of 4BBA in solution indicate slight variations in the electronic structure of protonated and deprotonated forms of 4BBA. The redshift, observed as pH increases, occurs at the reported pKa of 4BBA, suggesting that deprotonation plays a role in the absorbance spectral shift. These variations may alter the solvating effects and stability of 4BBA, as well as its optical properties in the aqueous phase.

Comparison of experimental results with theoretical calculations

As noted above, the experimental spectrum of 4BBA at pH=1 shows two bands: a strong I-band at 260 nm and a weak broad II-band between 320-360 nm (**Figure 2**). However, the spectrum at high pH has only one strong I-band centered at 264 nm. Above pH 4, the I-band on the UV-Vis spectra of aqueous 4BBA is redshifted by 4 nm and becomes significantly intense with increasing pH. The ratio of experimental I-bands intensities between pH 1 and 6, pH values that represent the theoretical models, is $\frac{I_{pH=1}}{I_{pH=6}} = 0.84$.

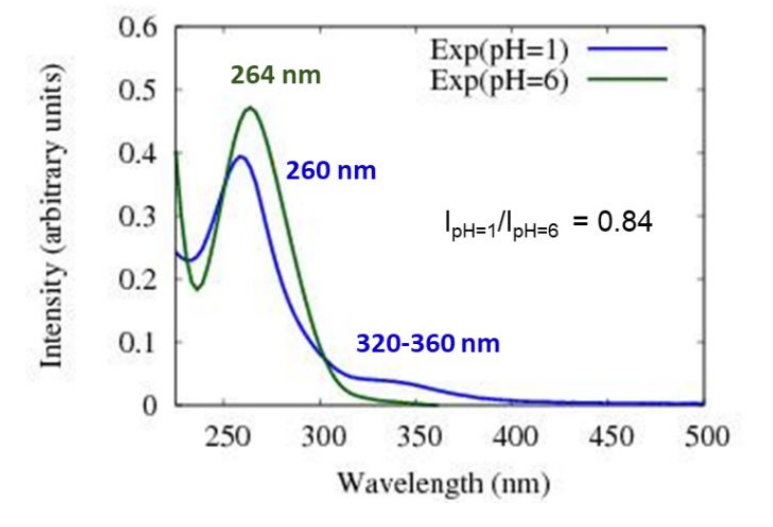


Figure 3. Experimental UV-Vis absorption spectra of 4BBA at both pH = 1 (blue line) and pH=6 (green line). These two spectra were used to compare theoretical results of protonated and deprotonated 4BBA.

Spectral changes in aqueous 4BBA with respect to pH, summarized in Figure 3, suggest that the increase in pH, with the concomitant deprotonation of 4BBA, results in two competing effects that ultimately lead to a slight redshift of the I-band: First, the electron delocalization of the deprotonated species (higher pH) decreases the electron transition energy, leading to a redshift in the absorption spectrum as pH increases. Second, the interaction between water and the more polar anionic 4BBA is relatively more favorable, which stabilizes the ground state of the deprotonated species (higher pH) compared to that of neutral species (lower pH). This last solvent effect increases the electron transition energy, resulting in a slight blueshift. This last effect is not as significant, leading to an overall redshift with pH increase. Understanding the relative magnitude of these two competing effects is examined using theoretical clusters (vide infra). Yet, experimental results suggest that the relatively low solubility of 4BBA, interpreted here as a less favored interaction between water and 4BBA compared to smaller organic acids, minimizes the second effect, leading primarily to a redshift in the absorption spectrum as pH increases due primarily to electron delocalization. Water interaction with 4BBA, even though smaller than other organic acids, are enough to counterbalance the redshift due to delocalization, resulting in only a slight redshift as pH increases, shown in Figures 2 and 3. The relative combination of these two competing effects is more complex, as it involves 4BBA speciation, energy changes in the excited state, and the intermolecular interaction of each speciated form with water molecules. Overall, the small redshift observed in 4BBA solutions indicates that the electronic structure of the anions and neutral species are relatively similar.

Using the DFT method, we calculated the populations of the keto- and diol-forms of 4BBA in a water solution at various pH values by evaluating the free Gibbs energy change between these forms (see **Fig. S3a-b, SI**). Our results revealed that the keto-form is energetically favored in both cases, with ΔG values of -8.31 kcal/mol for the neutral state and -13.69 kcal/mol for the ionized state. Consequently, at room temperature in low pH water, it is expected that the neutral keto-form will dominate (91.76%), while the neutral diol-form will constitute a smaller fraction (8.24%). Similarly, at high pH, the ionized keto-form is expected to be overwhelmingly predominant (99.98%), while the ionized diol-form will be present in negligible quantities (0.02%). These findings provide valuable insights into the relative populations of the different forms of 4BBA under specific pH conditions.

Small theoretical clusters - 4BBA·(H₂O)₈. Experimental results suggest that the keto-form is the primary species in the acid-base aqueous equilibrium of 4BBA. To confirm this observation and to reproduce the two bands observed in the 4BBA solution at pH 1.0, theoretical complexes of neutral keto- and the diol-forms of 4BBA were used as possible models of 4BBA at low pH. The comparison between the experimental optical absorption spectrum at pH=1 and two theoretical models are presented in Figure 4a and 4b, for the neutral keto-form and the neutral diol-form, respectively. The small cluster model of the neutral keto-form of 4BBA simulating low pH speciation exhibits two bands, similar to the experimental observation: a strong I-band and low-

energy broad II-bands (Fig. 4a).

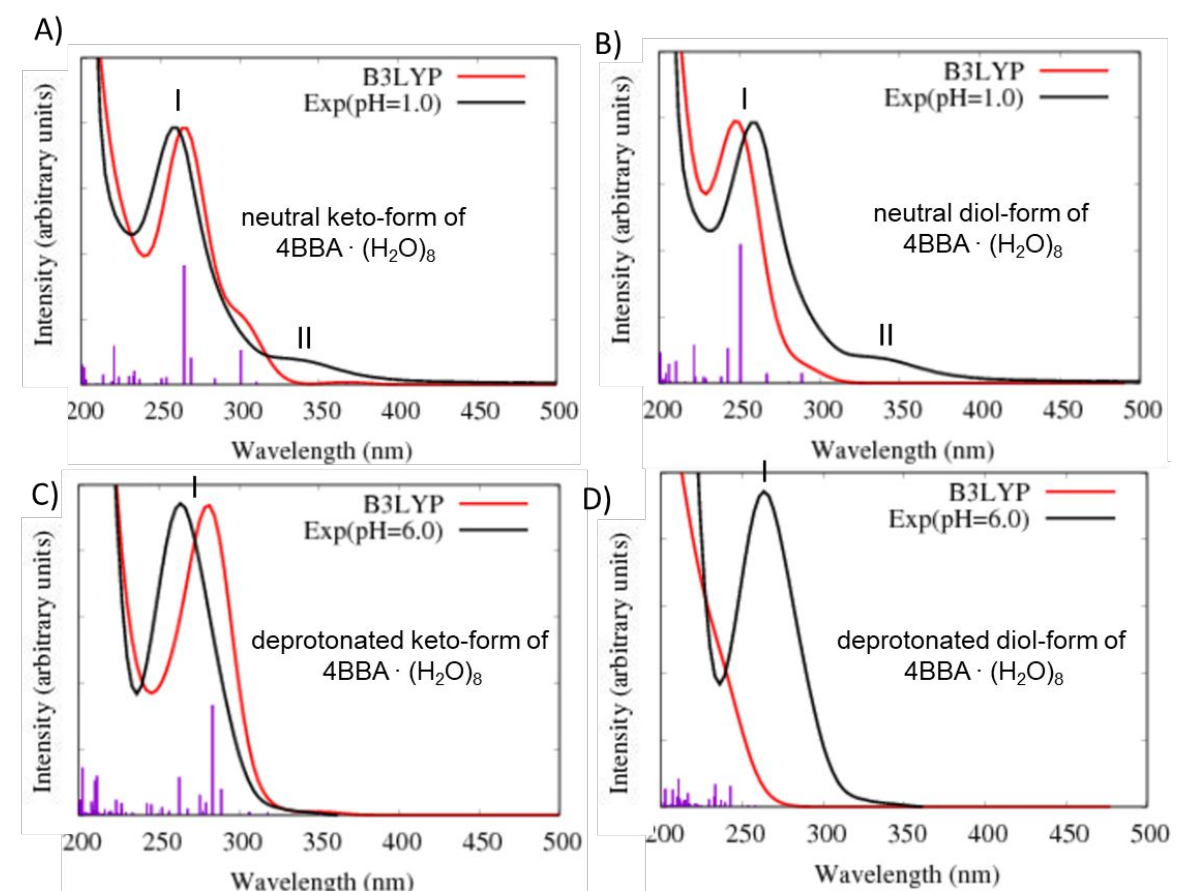


Figure 4. Comparison of the theoretical (red line) and experimental (black line) optical absorption spectra at different pH. Level of theory is B3LYP/6-311++G** (gas phase).

In the theoretical spectrum of neutral keto-4BBA, the strong band at 265 nm can be considered as the experimental I-band and the second broad low-energy band at 300 nm can be assigned with the experimental II-band. This small cluster model provides reasonable agreement between experiment and theory in the case of strong I-band, with a difference in the peak position between theory and experiment of 5 nm. However, according to the theoretical results, the experimental II-band appeared at significantly lower wavelengths (Table 1). Additional solvent effects, such as the polarizable continuum model (C-PCM) do not make any significant improvements in the calculation (Fig. S4, SI).

Calculation of the optical spectrum for the neutral keto-form of 4BBA·(H₂O)₈ using different functionals, including CAM-B3LYP, LRC-wPBEh, and wB97X, revealed their inability to reproduce the low-energy band accurately (**Fig. S5a, SI**). This is consistent with our previous studies on benzoic acid (BA) at low pH, where the low-energy band was also challenging to reproduce using TD-DFT. In contrast, the ADC(2) method successfully reproduced the intensities and position of the peaks of the BA spectrum, with good agreement between theory and experiment (**Fig. S5b, SI**). Despite the fact that ADC(n) level of theory was able to address these issues, its computational demand makes it impractical for the current system. Also, it is important to note that in the study of benzoic acid (BA), TD-DFT could accurately reproduce the nature of the involved orbitals for both bands, achieving a level of accuracy comparable to the more advanced ADC(2) method (**Fig. S5b, SI**). Therefore, in the current work, we can confidently conclude that the theoretical broad low-energy band observed in the spectrum of the neutral keto-4BBA is indeed related to the II-band observed in the experimental spectrum. This suggests that TD-DFT can capture the electronic characteristics of the excited states involved in this specific system.

The optical spectrum of neutral diol-form also exhibits two spectral bands at 251 and 289 nm (**Fig. 4b, Table 1**). However, the difference with experimental data is more significant with comparison to the keto-form: the I-band of this theoretical spectrum is blue-shifted 9 nm and the II-band is shifted 51 nm. The experimental energy gap between these two bands is around 1.1 eV, whereas the theoretical calculation yields a significantly smaller value of 0.65 eV (**Table 1**).

Two additional models were considered to simulate the optical spectrum of 4BBA at high pH: deprotonated keto- and diol-forms of 4BBA with 8 water molecules. The shape of the theoretical spectrum of the deprotonated keto-form of 4BBA is in good agreement with experimental results (**Fig. 4c, Table 1**). However, the calculated spectrum of the deprotonated diol-form of 4BBA exhibits a shoulder band blue-shifted with respect to the experimental peak II

. There is only a weak shoulder band above 250 nm (**Fig. 4d**). Calculated spectra for four speciated forms of 4BBA allowed us to conclude that molecule of 4BBA at pH=1 exists in neutral ketoform, whereas at pH=6 it should have a deprotonated keto-structure. These theoretical results agree with the experimental findings and further suggest that the hydrate form of 4BBA is not present in aqueous phase.

The orbitals involved in the electron transitions in both protonated and deprotonated clusters are shown in **Figure 5** and **6**. The low-energy II-band of the neutral keto-form arises due to the $\pi \rightarrow \pi^*$ transitions (**Fig. 5**). However, the strong I-band appearances due to the mixture of $n \rightarrow \pi^*$ and $\pi \rightarrow \pi^*$ transitions for both speciated forms: neutral- and deprotonated keto-4BBA (**Fig. 5** and **6**).

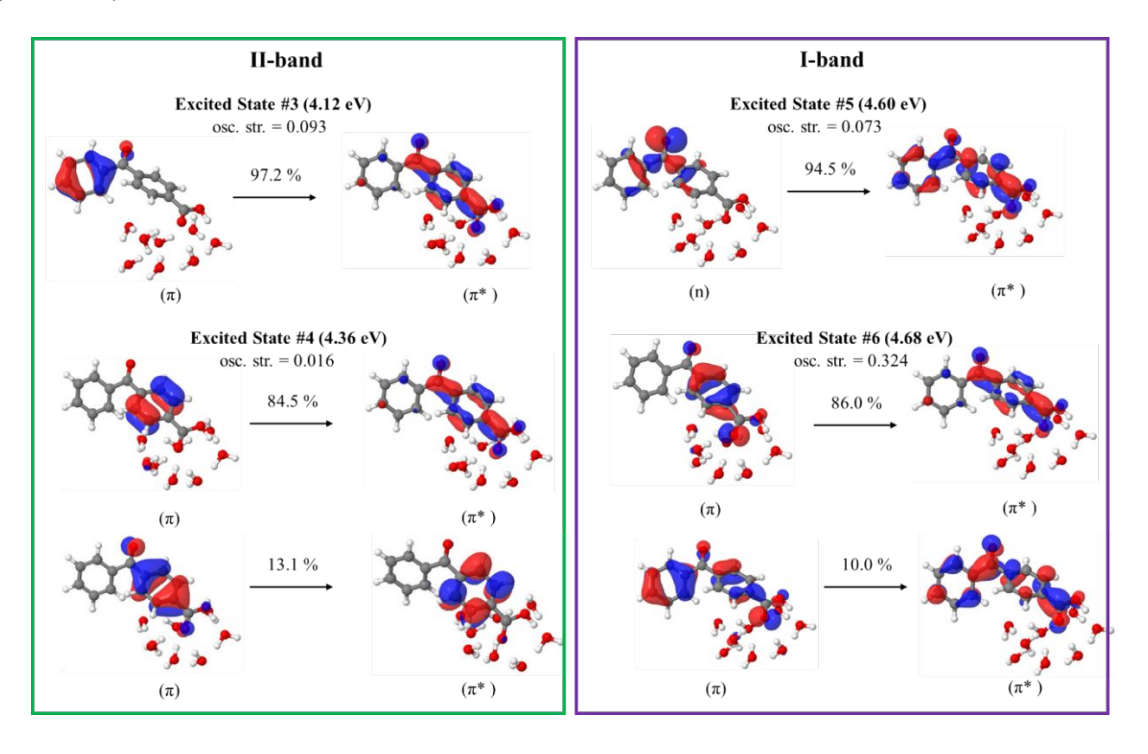


Figure 5. Natural transition orbitals of the selected excited states of neutral keto-form of $4BBA \cdot (H_2O)_8$ calculated at the B3LYP/6-311++G** (gas phase).

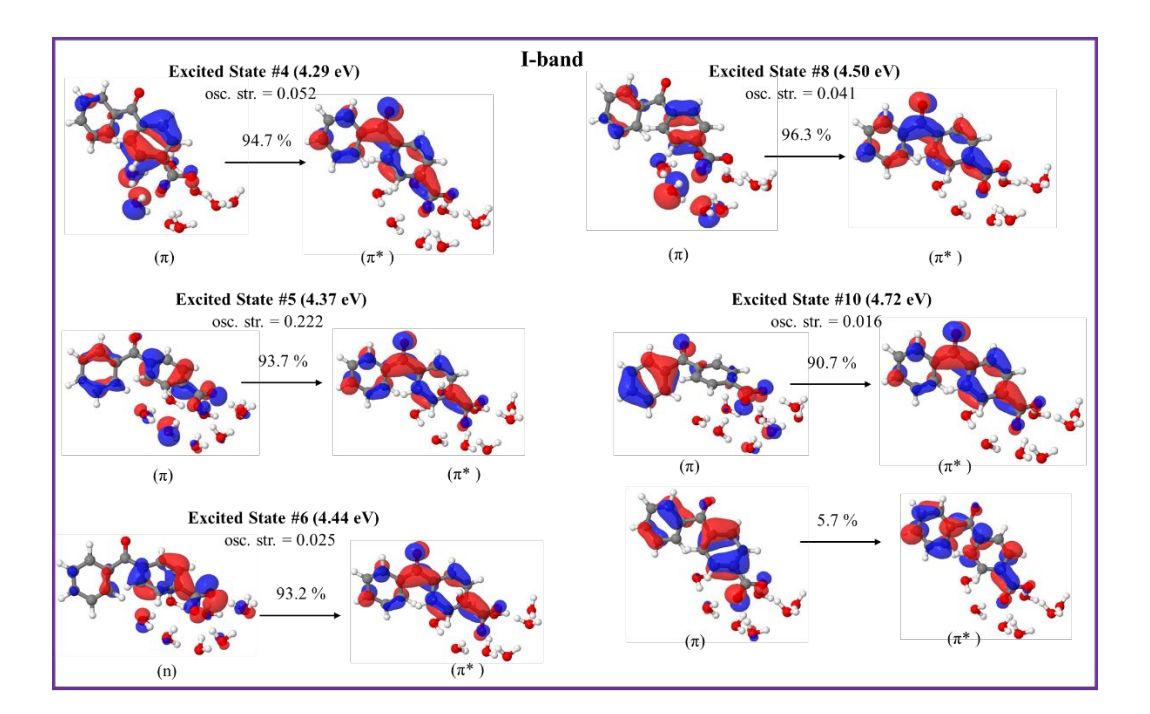


Figure 6. Natural transition orbitals of the selected excited states of deprotonated keto-form of 4BBA·(H₂O)₈ calculated at the B3LYP/6-311++G** (gas phase).

Comparison of orbitals corresponding to the neutral and deprotonated keto-clusters indicate clear similarities. For example, the I-band of both structures arises due to the mixture of $n\rightarrow\pi^*$ and $\pi\rightarrow\pi^*$ transitions (**Fig. 5** and **6**). However, there are certain differences that impact the spectral features of aqueous 4BBA. In particular, the natural transition orbitals (NTOs) of deprotonated structure located on the entire 4BBA fragment, whereas in the case of the neutral keto-form these orbitals are only located on the C_6H_5 -C(=O)- or C_6H_4 -COO fragments only (**Figure 5** and **6**). Additionally, we can see that orbitals on the water molecules participate in the electron transitions of the I-band of both neutral- and the deprotonated keto-forms of 4BBA. This suggests that both the organic acid and water molecules within the cluster contribute to excitation and further emphasizes the relevance of water cluster modeling around the chromophore. Thus, it is paramount to examine the effect of water solvation on the optical properties of 4BBA.

Calculated NTOs for the neutral keto-form of 4BBA·(H₂O)₈ using CAM-B3LYP/6-311++G** level of theory can be found in **Figure S6**, **SI**. The results obtained from both B3LYP and CAM-B3LYP functionals exhibit striking similarity, with all Highest Occupied Molecular Orbitals (HOMOs) and Lowest Unoccupied Molecular Orbitals (LUMOs) being localized solely on the 4BBA molecules. Notably, there are no orbitals involving the water molecules, indicating the absence of any detected charge transfer process.

Large water clusters - $4BBA \cdot (H_2O)_{30}$. The experimental data and DFT population analysis based on Gibbs energy indicated that the keto-form of 4BBA is the dominant species at low and high pHs. Presented TD-DFT results for the small models reproduce the agreement with the experiment well. However, despite the success achieved with small model systems for other chromophores, 1,36 the solvent effects cannot be fully reproduced for aqueous phase 4BBA using just 8 water molecules, as the solvent interactions are limited to the carboxylic acid group. Therefore, larger water clusters are necessary to simulate the interactions of the carboxy-, keto- and diol-groups of the 4BBA system with water. To achieve this level of interactions between water and all functional groups within the 4BBA molecule, larger clusters of 30 water molecules were simulated. To consider the contribution to the total optical absorption spectrum of all possible speciated forms, MD-DFTB trajectories were simulated and used to calculate the total TD-DFTB optical absorption spectrum of the largest systems. It is important to mention that our comparative analysis of the optical absorption spectra using the TD-DFTB and TD-DFT methods demonstrated good agreement, particularly for the neutral systems (Fig. S2). This suggests that the observed differences in the optical spectra between small systems calculated with TD-DFT and large systems calculated with TD-DFTB along the MD-DFTB trajectories can be attributed to solvent effects and the contribution of different speciated forms.

The optical spectra of the neutral forms of 4BBA (low pH models) were found to be significantly influenced by the contribution of different speciated forms and solvent effects, as evidenced by the results obtained for larger clusters $4BBA \cdot (H_2O)_{30}$ (**Figure 7a-b**). In Figure 7a, we can see some improvements in the theoretical spectrum of neutral keto-form of $4BBA \cdot (H_2O)_{30}$ related to the position of the low-energy II-band. This band still has a higher amplitude than it has in the experiment, but the position of this band is closer to the experiment. The gap between the I and II peaks is closer to the experimental value for the larger complexes (**Table 1**).

The optical spectrum of the neutral diol form of 4BBA, calculated with 30 water molecules, exhibits a distinct feature not observed in the spectrum obtained with eight water molecules: the intensity of the low-energy broad peak (II-band between 325 - 375 nm) increases in the presence of the larger water cluster (Fig. 7b). Additionally, the energy gap between I- and II-bands became larger, around 1.0 eV. This result is likely due to solvating stabilization of the diol-forms, which can form hydrogen bonding with water molecules in the geminal diol carbon. The separation between the carbonyl and the hypothetical diol functional groups in the neutral diol-form of 4BBA prevents the formation of intramolecular hydrogen bonding, leaving the diol-form and carbonyl groups available for intermolecular hydrogen-bonding with the water solvent. This effect is in stark contrast with smaller environmentally relevant chromophores, such as pyruvic acid, where intermolecular interactions tend to stabilize the protonated forms and weaken intermolecular hydrogen bonding with the surrounding water. 35 This intramolecular H-bonding likely contributes to the stability of the diol-form of keto-acids in solution, the effect absents in 4BBA. This lowenergy band on the spectrum of the neutral diol-form of 4BBA·(H₂O)₃₀ is very close (position and size of magnitude) to the experimental II-band of 4BBA at low pH.

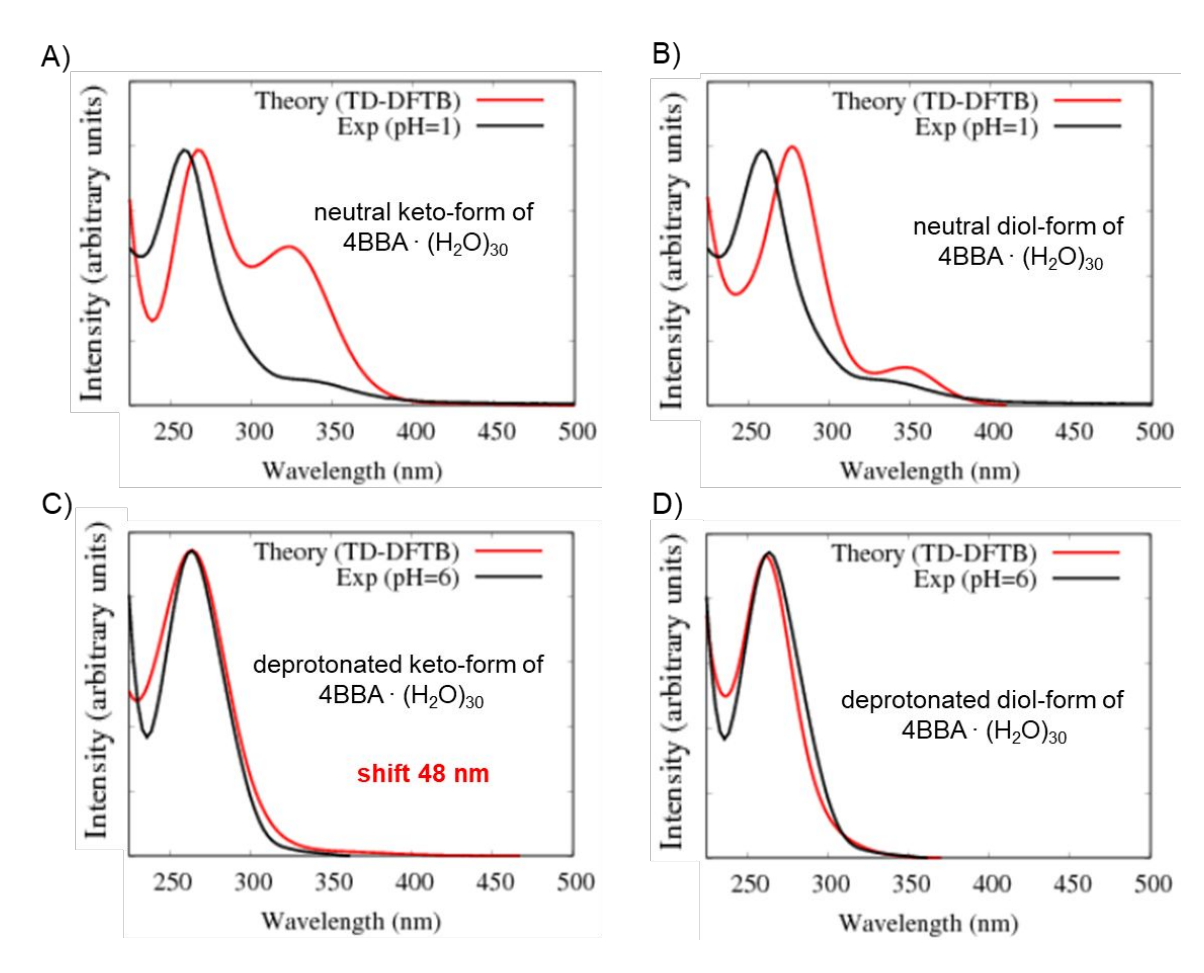


Figure 7. Comparison of the theoretical (red line) and experimental (black line) optical absorption spectra at low pH. The theoretical spectrum is an average spectrum of all structures along MD-DFTB trajectories. The level of theory is TD-DFTB.

Table 1. Experimental and theoretical optical absorption spectral data for 4BBA at different pH

Two is an arrangement of the state of the st					
Bands	Experiment	TD-DFT		TD-DFTB	
	(pH=1)	neutral 4BBA·(H ₂ O) ₈		neutral 4BBA·(H ₂ O) ₃₀	
		keto-form	diol-form	keto-form	diol-form
I-band	260 nm	265 nm	251 nm	267 nm	274 nm
	4.77 eV	4.68 eV	4.94 eV	4.64 eV	4.53 eV
II-band ^s	320 -360 nm	300 nm	289 nm	315-375 nm	325-375 nm
	3.44-3.89 eV	4.13 eV	4.29 eV	3.31-3.94 eV	3.31-3.82
Bands	Experiment	TD-DFT		TD-DFTB	
	(pH=6)	deprotonated 4BBA·(H ₂ O) ₈		deprotonated 4BBA·(H ₂ O) ₃₀	
		keto-form	diol-form	keto-form	diol-form
I-band	264 nm	283 nm	< 250 nm	309 nm	261 nm
	4.67 eV	4.38 eV	>4.96 eV	4.01 eV	>4.74 eV

Open Access Article. Published on 05 June 2023. Downloaded on 6/13/2023 4:50:28 PM.

This article is licensed under a Creative Commons Attribution-NonCommercial 3.0 Unported Licence

The optical spectra of the deprotonated keto-form complexes (high pH models) exhibited a noticeable redshift compared to both the experimental data and the small water cluster system (**Table 1**). However, the overall shape of the theoretical curve closely matches the experimental results. Despite the I-band centered at a higher wavelength than the experimental band, it is consistent with the redshift experimentally observed upon pH increase across the pKa of 4BBA (**Fig. 7c**). This matching behavior from protonated to deprotonated forms suggests that 4BBA at pHs above the pKa exists in deprotonated keto-form, in good agreement with the experimental findings. Overall, there is a 48 nm difference between experimental and theoretical spectra of the deprotonated keto-forms due to the increasing effect of solvating water molecules in the deprotonated 4BBA, demanding more challenging computation. This significant spectral shift of the theoretical spectra of 4BBA complexes in the keto-form with respect to the experimental data can be related to the relatively short MD trajectories where the system did not have enough time for relaxation. Thus, extending the molecular dynamics trajectories should increase the agreement between theoretical simulations and experimental observations where the system will reach a more stable and equilibrated state.

In contrast to the small cluster, the calculated spectrum of the deprotonated diol-form of 4BBA·(H₂O)₃₀ exhibits a strong peak at 261 nm (**Fig. 7d**). The peak of the large cluster has stronger intensity and it is red-shifted compared to the small cluster. This phenomenon can be attributed to solvent effects, specifically the interaction between water molecules and the diol group, which leads to a stabilization of the diol-form of 4BBA..

The structures of all speciated forms of 4BBA were initially placed at the center of a 30-water cluster sphere. Diol- and keto-forms exhibit different water distribution distributions during the MD simulations. In the case of the keto-forms (**Fig. 8a-b**), the keto-group coordinates with just

1 or 2 water molecules. For the neutral keto-structure, there are 60% of trajectories lead to the formation of structures with two water molecules coordinated nearby the keto-group (**Fig.8 a.2-3**), whereas, in the case of deprotonated form, there are 90% of all trajectories where just one water molecule is located near the oxygen of keto-group (**Fig.8 b.2-3**). The opposite is found for the diolforms, the diol-functional group increases the capability of hydrogen bonding with surrounding water molecules compared to the keto-group. A strong diol-group and water molecules interaction is observed (**Fig.8 c-d**). Given the additional OH functional group in the geminal carbon, the diolgroup coordinates with 3 or 4 water molecules with an average hydrogen bond distance of 2 Å (**Fig.8 c-d**). These hydrogen-bond lengths do not significantly change during the MD simulation time (**Fig.8 c.3, d.3**).

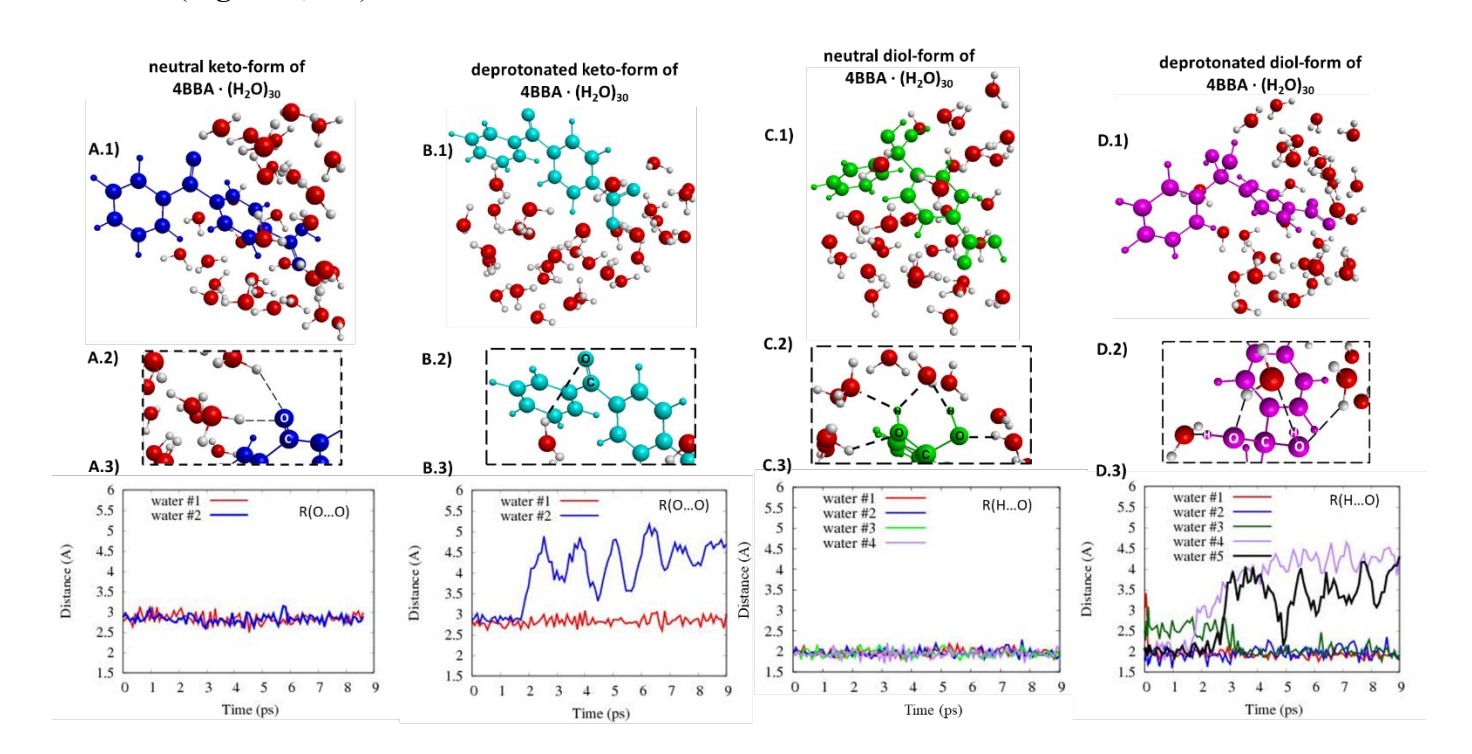


Figure 8. Selected structures of (A.1) neutral keto-form of 4BBA; (B.1) deprotonated keto-form of 4BBA; (C.1) neutral diol-form of 4BBA; (D.1) deprotonated diol-form of 4BBA; (A.2, B.2, C.2, D.2) water molecules coordination around keto- and diol- groups. Distances between the oxygen atom of keto-group and oxygen atoms of nearest water molecules (along MD trajectory) for neutral (A.3) and deprotonated (B.3) clusters of keto-form 4BBA. Hydrogen bonds along MD trajectory between the diol-group and nearest water molecules in the cluster of neutral diol-form of 4BBA (C.3) and deprotonated diol-form of 4BBA (D.3). **Note**: for the keto-form, we considered

O...O distances, because some of the water molecules using different hydrogen atoms to coordinate by an oxygen atom of keto-group along the trajectory.

Overall, theoretical calculations and experimental findings indicate that the experimental optical spectra of aqueous phase 4BBA at low pH can be represented by the neutral keto-form. Similarly, the theoretical spectrum of deprotonated keto-form successfully represents experimental spectra at high pH, as it models the experimentally observed redshift that takes as pH increases. Calculations confirm that the more electron-delocalized deprotonated keto-form form of 4BBA, observed at higher pHs, leads to a small decrease in the excitation energy observed as a redshift in **Figure 1**. In contrast, the deprotonated keto-form leads to a shift to the blue as pH increases, likely due to water interactions. While the theoretical spectrum of the deprotonated keto-form form of 4BBA models the correct direction of the spectral shift with respect of pH, a more accurate simulation of water solvent effects at different pH is needed to improve the agreement between theory and experiment further.

Conclusions

Chromophoric organic acids containing aromatic groups are widely present in the sea surface and can partition into the atmosphere through bubble bursting and wave breaking.^{19, 37} Thus, these chromophores can undergo significant pH changes, from the slightly basic sea surface microlayer (SSML pH 7.8) to the more acidic sea spray aerosol (SSA pH 2 to 4).⁴⁶ Molecules like 4BBA, often used as a proxy of more complex organic substances, such as CDOM and humic-like substances, can provide molecular level understanding of light-induced environmental processes and the role of chromophores in the Earth's radiative energy balance.^{5, 40-43} Therefore, the systematic investigation of 4BBA absorption carried out here provides critical understanding of

the optical properties as it is applied to represent more complex light absorbing substances in specific environmental conditions.

In the present work, spectroscopic measurements are combined with theoretical calculations to study the optical absorption spectra of 4BBA in an aqueous solution. ¹H-NMR spectra were used to experimentally determine that no hydration diol-forms of 4BBA are detectable at the pHs examined, indicating that the speciation of aqueous phase 4BBA consists on keto-forms. These experimental data, combined with potentiometric titrations, were used to determine the pKa of 4BBA at 3.41±0.04. The theoretical hydrated model agrees well with the experimental spectra, especially for neutral speciated forms. Calculated absorption spectra also indicate that the keto-forms of 4BBA are the predominant form of 4BBA in the aqueous phase. Overall, the work shown here suggests that 4BBA, when used as a moiety of environmental photosensitizers, has characteristic speciation and optical properties depending on the pH of the environment, primarily as a protonated keto-form when present in SSA to the deprotonated ketoform in SSML and bulk natural waters. For these calculations, solvent effects are an important parameter for reproducing the correct optical spectra of 4BBA in the water environment, especially at low pH. Our theoretical results agree with experimental observations, with lower pH I-band showing both experimentally (at 260 nm) and theoretically (at 265 nm, TD-DFT). At higher pHs, the effect of water becomes weaker, with the redshift upon pH increase at 4 nm experimentally and 18 nm (TD-DFT) in our simulation.

Experimental optical spectra of 4BBA at different pH can be presented by the neutral ketoform in the case of low pH and deprotonated keto-form in the case of high pH. Both experimental and theoretical results indicate the presence of a high-energy I-band that undergoes a slight redshift as pH increases, moving it closer to the solar spectral region. In addition, a low energy II-band at

Open Access Article. Published on 05 June 2023. Downloaded on 6/13/2023 4:50:28 PM

330 nm only shows at low pHs characteristic of sea spray aerosols. Theoretical model clusters of 4BBA with different numbers of water molecules demonstrated that solvent effects are crucial in reproducing the correct optical spectra of 4BBA. Theoretical clusters can be successful in describing chromophores in solution. Theoretical results showed that the I-band of both speciated forms of 4BBA arises from the combination of $n \rightarrow \pi^*$ and $\pi \rightarrow \pi^*$ transitions. Orbital analysis of the theoretical clusters allowed us to see that the orbitals involved in the electron transitions of the I-band involve a combination of 4BBA and water molecules within the cluster. Combining quantum chemical calculations of excited states with molecular dynamics thoroughly interprets experimental results and demonstrates the possibility of microscopic insight into the absorption spectra of organic molecules in water by calculations restricted to cluster models. The results show that a good spectroscopic description of organics dissolved in bulk can be obtained by simulations for clusters of water of moderate sizes. It seems sufficient when the waters roughly extend over the size of the organic species. Applications to other systems of this type should thus be feasible.

Supporting Information

The Supporting Information is available on the PCCP website. Additional data related to this paper can be accessed from the NSF-CAICE Data Repository (doi: PENDING) or may be requested from the authors.

Acknowledgments

The authors would like to thank Mark Young and Imon Mandal for helpful comments, Anthony Mrse for assistance with NMR spectra analysis, and Alma Montserrat Palacios Puga and Gilberto Daniel Partida Coria for solution preparation in the ¹H-NMR experiments. The authors would like to gratefully acknowledge support from the National Science Foundation through the Center for Aerosol Impacts on Chemistry of the Environment funded under the Centers for Chemical Innovation Program Grant CHE1801971. Additionally, this work used the Extreme Science and Engineering Discovery Environment (XSEDE),⁷¹ and SDSC EXPANSE CPU through allocations from the Advanced Cyberinfrastructure Coordination Ecosystem: Services & Support (ACCESS) program, which is supported by grant number TG-CHE170064 and the MERCURY consortium (http://mercuryconsortium.org/) under NSF grants CHE-1229354 and CHE-1662030.

References

- 1. N. Karimova, M. Luo, V. H. Grassian, R. Gerber. Absorption Spectra of Benzoic Acid in Water at Different pH and in the Presence of Salts: Insights from the Integration of Experimental Data and Theoretical Cluster Models. Phys. Chem. Chem. Phys. 2020, 22, 5046-5056.
- 2. E. M. Thurman. Organic Geochemistry of Natural Waters; Springer: Netherlands, Dordrecht, **1985**.
- 3. J. Borgatta, J. G. Navea. Fate of Aqueous Iron Leached from Tropospheric Aerosols during Atmospheric Acidic Processing: Study of the Effect of Humic-Like Substances. WIT Trans. Ecol. Environ. 2015, 198, 155-166.
- 4. Drapanauskaite, D.; Buneviciene, K.; Repsiene, R.; Mazeika, R.; Navea, J.; Baltrusaitis, J. Physicochemical Characterization of Pelletized Lime Kiln Dust as Potential Liming Material for Acidic Soils. Waste and Biomass Valorization 2020.
- 5. S. L. Mora Garcia, S. Pandit, J. G. Navea, V. H. Grassian. Nitrous Acid (HONO) Formation from the Irradiation of Aqueous Nitrate Solutions in the Presence of Marine Chromophoric Dissolved Organic Matter: Comparison to Other Organic Photosensitizers. ACS Earth Space Chem. **2021**, 5, 11, 3056–3064.
- 6. Ricker, H. M.; Leonardi, A. L.; Navea, J. G. Reduction and Photoreduction of NO₂ in Humic Acid Films as a Source of HONO, ClNO, N₂O, NO_X, and Organic Nitrogen. ACS Earth *Space Chem.* **2022**, 6, 12, 3066–3077.
- 7. K. Mopper, R. G. Zika. Natural Photosensitizers in Sea Water: Riboflavin and Its Breakdown Products. In Photochemistry of Environmental Aquatic Systems. American Chemical Society. 1987; 327, 174-190.
- 8. D. J. Hassett, M. S. Bisesi, R. Hartenstein. Bactericidal action of humic acids. Soil Biol. Biochem. 1987, 19, 111-113.

- 9. M. A. Young. Environmental Photochemistry in Surface Waters. In *Water Encyclopedia* (eds J.H. Lehr and J. Keeley). Wiley. **2005**, 529-535.
- 10. M. Klavins, O. Purmalis. Humic substances as surfactants. *Environ. Chem. Lett.* **2010**, *8*, 349-354.
- 11. J. A. Rice, P. MacCarthy. Statistical evaluation of the elemental composition of humic substances. *Org. Geochem.* **1991**, *17*, 635-648.
- 12. C. E. J. van Rensburg. The Antiinflammatory Properties of Humic Substances: A Mini Review. *Phytother. Res.* **2015**, *29*, 791-795.
- 13. M. Zark, T. Dittmar. Universal molecular structures in natural dissolved organic matter. *Nature Comm.* **2018**, *9*, 3178.
- 14. W. S. Wan Ngah, M. A. K. M. Hanafiah, S. S. Yong. Adsorption of humic acid from aqueous solutions on crosslinked chitosan–epichlorohydrin beads: Kinetics and isotherm studies. *Coll. Surf. B: Biointerfaces.* **2008**, *65*, 18-24.
- 15. D. Kwon, M. J. Sovers, V. H. Grassian, P.D. Kleiber, M. A. Young. Optical Properties of Humic Material Standards: Solution Phase and Aerosol Measurements. *ACS Earth Space Chem.* **2018**, *2*, 1102-1111.
- S. Jayalath, H. Wu, S. C. Larsen, V. H. Grassian. Surface Adsorption of Suwannee River Humic Acid on TiO2 Nanoparticles: A Study of pH and Particle Size. *Langmuir* 2018, 34, 3136-3145.
- 17. Y. Miyazaki, Y.; Yamashita, Y.; Kawana, K.; Tachibana, E.; Kagami, S.; Mochida, M.; Suzuki, K.; Nishioka, J. Chemical transfer of dissolved organic matter from surface seawater to sea spray water-soluble organic aerosol in the marine atmosphere. *Scientific Reports.* **2018**, *8*, 14861.
- 18. M. V. Santander, J. M. Schiffer, C. Lee, J. L. Axson, M. J. Tauber, K. A. Prather, Factors controlling the transfer of biogenic organic species from seawater to sea spray aerosol. *Scientific Reports.* **2022**, *12*, 3580.
- J. V. Trueblood, M. R. Alves, D. Power, M. V. Santander, R. E. Cochran, K. A. Prather, V. H. Grassian. Shedding Light on Photosensitized Reactions within Marine-Relevant Organic Thin Films. ACS Earth Space Chem. 2019, 3, 1614-1623.
- 20. K. McNeill, S. Canonica. Triplet state dissolved organic matter in aquatic photochemistry: reaction mechanisms, substrate scope, and photophysical properties. *Environ. Sci.: Processes Impacts.* **2016**, *18*, 1381-1399.
- 21. C. Baduel, D. Voisin, J.-L Jaffrezo. Seasonal variations of concentrations and optical properties of water soluble HULIS collected in urban environments. *Atm. Chem. Phys.* **2010**, 10, 4085–4095

- 22. A. Hoffer, A. Gelencsér, P. Guyon, G. Kiss, O. Schmid, G. P. Frank, P. Artaxo, M. O. Andreae. Optical properties of humic-like substances (HULIS) in biomass-burning aerosols. Atmos. Chem. Phys. **2006**, 6, 3563-3570.
- 23. Y. Chin, G. Aiken, E. O'Loughlin. Molecular Weight, Polydispersity, and Spectroscopic Properties of Aquatic Humic Substances. Environ. Sci. Technol. 1994, 28, 1853-1858.
- 24. D. P. Veghte, S. China, J. Weis, L. Kovarik, M. K. Gilles, A. Laskin. Optical Properties of Airborne Soil Organic Particles. ACS Earth Space Chem. 2017, 1, 511-521.
- 25. K. Kumada. Absorption spectra of humic acids. Soil Sci. Plant Nutr. 1955, 1, 29-30.

Open Access Article. Published on 05 June 2023. Downloaded on 6/13/2023 4:50:28 PM

- 26. X. Lei, J. Pan, A. Devlin. Characteristics of Absorption Spectra of Chromophoric Dissolved Organic Matter in the Pearl River Estuary in Spring. Remote Sensing 2019, 11, 3 1533.
- 27. J. Ma, R. Del Vecchio, K. S. Golanoski, E. S. Boyle, N. V. Blough. Optical Properties of Humic Substances and CDOM: Effects of Borohydride Reduction. Environ. Sci. Technol. **2010**, 44, 5395-5402.
- 28. E. S. Boyle, N. Guerriero, A. Thiallet, R. D. Vecchio, N. V. Blough. Optical Properties of Humic Substances and CDOM: Relation to Structure. Environ. Sci. Technol. 2009, 43, 2262-2268.
- 29. M. Peacock, C. Evans, N. Fenner, C. Freeman, R. Gough, T. Jones, I. Lebron. UV-visible absorbance spectroscopy as a proxy for peatland dissolved organic carbon (DOC) quantity and quality: Considerations on wavelength and absorbance degradation. *Environ. Science*: Processes & Impacts 2014, 16, 1445-1461.
- 30. H. E. Reader, C. A. Stedmon, N. J. Nielsen, E. S. Kritzberg. Mass and UV-visible spectral fingerprints of dissolved organic matter: sources and reactivity. Frontiers in Marine Science **2015**, 2, 88.
- 31. A. Momzikoff, R. Santus, M. A. Giraud. A study of the photosensitizing properties of seawater. Mar. Chem. 1983, 12, 1-14.
- 32. A. Leonardi, H. M. Ricker, A. G. Gale, B. T. Ball, T. T. Odbadrakh, G. C. Shields, J. G. Navea. Particle formation and surface processes on atmospheric aerosols: A review of applied quantum chemical calculations. Int. J. Quantum Chem. 2020, e26350.
- 33. J. G. Navea, V. H. Grassian. Photochemistry of Atmospheric Particles. In Reference Module in Chemistry, Molecular Sciences and Chemical Engineering. Elsevier: 2017
- 34. N. V. Karimova, M. Luo, V. H. Grassian, B. R. Gerber. Towards a microscopic model of light absorbing complex organic components an aqueous environments: Theoretical and experimental study. Phys. Chem. Chem. Phys. 2021,23, 10487-10497

Open Access Article. Published on 05 June 2023. Downloaded on 6/13/2023 4:50:28 PM

- 35. C. J. Ostaszewski, N. M. Stuart, D. M. B. Lesko, D. Kim, M. J. Lueckheide, J. G. Navea. Effects of Coadsorbed Water on the Heterogeneous Photochemistry of Nitrates Adsorbed on TiO2. *J. Phys. Chem. A* **2018**, *122*, 6360-6371.
- 36. D. Shemesh, M. Luo, V. H. Grassian, R. B. Gerber. Absorption Spectra of Pyruvic Acid in Water: Insights from Calculations for Small Hydrates and Comparison to Experiment. *Phys. Chem. Chem. Phys.* **2020**, *22*, 12658-12670.
- 37. M. R. Alves, E. K. Coward, D. Gonzales, J. S. Sauer, K. J. Mayer, K. A. Prather, V. H. Grassian. Changes in light absorption and composition of chromophoric marine-dissolved organic matter across a microbial bloom. *Environ. Sci. : Processes Impacts* **2022**, *24*, 1923-1933.
- 38. M. Luo, D. Shemesh, M. N. Sullivan, M. R. Alves, M. Song, R. B. Gerber, V. H. Grassian. Impact of pH and NaCl and CaCl₂ Salts on the Speciation and Photochemistry of Pyruvic Acid in the Aqueous Phase. *J Phys Chem A* **2020**, *124*, 5071-5080.
- 39. N. V. Karimova, M. Luo, V. H. Grassian, R. B. Gerber. Absorption spectra of benzoic acid in water at different pH and in the presence of salts: insights from the integration of experimental data and theoretical cluster models. *Phys. Chem. Chem. Phys.* **2020**, *22*, 5046-5056.
- 40. L. Tinel, S. Rossignol, A. Bianco, M. Passananti, S. Perrier, X. Wang, M. Brigante, D. J. Donaldson, C. George. Mechanistic Insights on the Photosensitized Chemistry of a Fatty Acid at the Air/Water Interface. *Environ. Sci. Technol.* **2016**, *50*, 11041-11048.
- 41. P. Corral Arroyo, T. Bartels-Rausch, P.A. Alpert, S. Dumas, S. Perrier, C. George, M. Ammann. Particle-Phase Photosensitized Radical Production and Aerosol Aging. *Environ. Sci. Technol.* **2018**, *52*, 7680-7688.
- 42. K. Couch, F. Leresche, C. Farmer, G. McKay, F. Rosario-Ortiz. Assessing the source of the photochemical formation of hydroxylating species from dissolved organic matter using model sensitizers. *Environ. Sci.: Processes Impacts* **2022**, *24*, 102-115.
- 43. M. E. Monge, T. Rosenørn, O. Favez, M. Müller, G. Adler, A. Abo Riziq, Y. Rudich, H. Herrmann, C. George, B. D'Anna. Alternative pathway for atmospheric particles growth. *Proc. Natl. Acad. Sci.* **2012**, *109*, 6840-6844.
- 44. H. E. Ungnade, R. W. Lamb. The Absorption Spectra of Benzoic Acid and Esters. *J. Am. Chem. Soc.* **1952**, *74*, 3789-3794.
- 45. Kamath, B. V.; Mehta, J. D.; Bafna, S. L. Ultraviolet absorption spectra: Some substituted benzoic acids. *J. Appl. Chem.* **1975**, *25*, 743-751.
- 46. K. J. Angle, D. R. Crocker, R. M. C. Simpson, K. J. Mayer, L.A. Garofalo, A. N. Moore, S. L. Mora Garcia, V. W. Or, S. Srinivasan, M. Farhan, J. S. Sauer, C. Lee, M. A. Pothier, D. K. Farmer, T. R. Martz, T. H. Bertram, C. D. Cappa, K. A. Prather, V. H. Grassian. Acidity

- across the interface from the ocean surface to sea spray aerosol. *Proc. Natl. Acad. Sci. USA* **2021**, 118, e2018397118.
- 47. C. R. Usher, A. E. Michel, V. H. Grassian. Reactions on mineral dust. *Chem. Rev.* 2003, 103, 4883-4940.
- 48. M. A. Freedman, E. E. Ott, K. E. Marak. Role of pH in Aerosol Processes and Measurement Challenges. J Phys Chem A 2019, 123, 1275-1284.
- 49. J. Borgatta, A. Paskavitz, D. Kim, J. G. Navea, Comparative evaluation of iron leach from fly ash from different source regions under atmospherically relevant conditions. *Environ*. Chem. 2016, 13.
- 50. D. M. B. Lesko, E. M. Coddens, H. D. Swomley, R. M. Welch, J. Borgatta, J. G. Navea. Photochemistry of nitrate chemisorbed on various metal oxide surfaces. Phys. Chem. Chem. Phys. 2015, 17, 20775-20785.

Open Access Article. Published on 05 June 2023. Downloaded on 6/13/2023 4:50:28 PM

- 51. D. Kim, Y. Xiao, R. Karchere-Sun, R.; E. Richmond, H. M. Ricker, A. Leonardi, J. G. Navea. Atmospheric processing of anthropogenic combustion particles: Iron mobility and nitrite formation from fly ash. ACS Earth Space Chem. 2020, 4, 750–761.
- 52. M. Luo, N. A. Wauer, K. J. Angle, A. C. Dommer, M. Song, C. M. Nowak, R. E. Amaro, V. H. Grassian. Insights into the behavior of nonanoic acid and its conjugate base at the air/water interface through a combined experimental and theoretical approach. Chem. Sci. **2020**, 11, 10647-10656.
- 53. Y. Shao, Z. Gan, E. Epifanovsky, A. T. B. Gilbert, M. Wormit, J. Kussmann, A. W. Lange, A. Behn, J. Deng, X. Feng, D. Ghosh, M. Goldey, P. R. Horn, L. D. Jacobson, I. Kaliman, R. Z. Khaliullin, T. Kuś, A. Landau, J. Liu, E. I. Proynov, Y. M. Rhee, R. Richard, M. A. Rohrdanz, R. P Steele, E. J. Sundstrom, H. L. Woodcock, P. M. Zimmerman, D. Zuev, B. Albrecht, E. Alguire, B. Austin, G. J. O. Beran, Y. A. Bernard, E. Berquist, K. Brandhorst, K. B. Bravaya, S. T. Brown, D. Casanova, C. Chang, Y. Chen, S. H. Chien, K. D. Closser, D. L. Crittenden, M. Diedenhofen, R. A. DiStasio, H. Do, A. D. Dutoi, R. G. Edgar, S. Fatehi, L. Fusti-Molnar, A. Ghysels, A. Golubeva-Zadorozhnaya, J. Gomes, M. Hanson-Heine, P. H. P. Harbach, A. W. Hauser, E. G. Hohenstein, Z. C. Holden, T. Jagau, H. Ji, B. Kaduk, K. Khistyaev, J. Kim, J. Kim, R. A. King, P. Klunzinger, D. Kosenkov, T. Kowalczyk, C. M. Krauter, K. U. Lao, A. D. Laurent, K. V. Lawler, S. V. Levchenko, C. Y. Lin, F. Liu, E. Livshits, R. C. Lochan, A. Luenser, P. Manohar, S. F. Manzer, S. Mao, N. Mardirossian, A. V. Marenich, S. A. Maurer, N. J. Mayhall, E. Neuscamman, C. M. Oana, R. Olivares-Amaya, D. P. O'Neill, J. A. Parkhill, T. M. Perrine, R. Peverati, A. Prociuk, D. R. Rehn, E. Rosta, M. J. Russ, S. M. Sharada, S. Sharma, D. W. Small, A. Sodt, T. Stein, D. Stück, Y. Su, A. J. W. Thom, T. Tsuchimochi, V. Vanovschi, L. Vogt, O. Vydrov, T. Wang, M. A. Watson, J. Wenzel, A. White, C. F. Williams, J. Yang, S. Yeganeh, S. R. Yost, Z. You, I. Y. Zhang, X. Zhang, Y. Zhao, B. R. Brooks, G. K. L. Chan, D. M. Chipman, C. J. Cramer, W. A. Goddard, M. S. Gordon, W. J. Hehre, A. Klamt, H. F. Schaefer, M. W. Schmidt, C. D. Sherrill, D. G. Truhlar, A. Warshel, X. Xu, A. Aspuru-Guzik, R. Baer, A. T. Bell, N. A. Besley, J. Chai, A. Dreuw, B. D. Dunietz, T. R. Furlani, S. R. Gwaltney, C. Hsu,

- Y. Jung, J. Kong, D. S. Lambrecht, W. Liang, C. Ochsenfeld, V. A. Rassolov, L. V. Slipchenko, J. E. Subotnik, T. Van Voorhis, J. M. Herbert, A. I. Krylov, P. M. W. Gill, M. Head-Gordon. Advances in molecular quantum chemistry contained in the Q-Chem 4 program package. *Mol. Phys.* **2015**, *113*, 184-215.
- 54. A. D. Becke. Density-functional thermochemistry. III. The role of exact exchange. *J. Chem. Phys.* **1993**, *98*, 5648-5652.
- 55. S. Grimme. Semiempirical GGA-type density functional constructed with a long-range dispersion correction. *J. Comput. Chem.* **2006**, *27*, 1787-1799.
- 56. T. N. Truong, E. V. A. Stefanovich. New method for incorporating solvent effect into the classical, ab initio molecular orbital and density functional theory frameworks for arbitrary shape cavity. *Chem. Phys. Lett.* **1995**, *240*, 253-260.
- 57. A. Bondi. van der Waals Volumes and Radii. *J. Phys. Chem.* **1964**, *68*, 441-451.
- 58. M. C. Almandoz, M. I. Sancho, S. E. Blanco. Spectroscopic and DFT study of solvent effects on the electronic absorption spectra of sulfamethoxazole in neat and binary solvent mixtures. *Spectrochimica Acta Part A: Molecular and Biomolecular Spectroscopy* **2014**, *118*, 112-119.
- 59. D. Porezag, T. Frauenheim, T. Köhler, G. Seifert, R. Kaschner. Construction of tight-binding-like potentials on the basis of density-functional theory: Application to carbon. *Phys. Rev. B* **1995**, *51*, 12947-12957.
- M. Gaus, Q. Cui, M. Elstner. DFTB3: Extension of the Self-Consistent-Charge Density-Functional Tight-Binding Method (SCC-DFTB). *J. Chem. Theory Comput.* 2011, 7, 931-948.
- 61. D. E. Romonosky, L. Q. Nguyen, D. Shemesh, T. B. Nguyen, S. A. Epstein, D. B. C. Martin, C. D. Vanderwal, R. B. Gerber, S. A. Nizkorodov. Absorption spectra and aqueous photochemistry of β-hydroxyalkyl nitrates of atmospheric interest. *Mol. Phys.* 2015, 113, 2179-2190.
- 62. B. Hourahine, B. Aradi, V. Blum, F. Bonafé, A. Buccheri, C. Camacho, C. Cevallos, M. Y. Deshaye, T. Dumitrică, A. Dominguez, S. Ehlert, M. Elstner, T. van der Heide, J. Hermann, S. Irle, J. J. Kranz, C. Köhler, T. Kowalczyk, T. Kubař, I. S. Lee, V. Lutsker, R. J. Maurer, S. K. Min, I. Mitchell, C. Negre, T. A. Niehaus, A. M. N. Niklasson, A, J. Page, A. Pecchia, G. Penazzi, M. P. Persson, J. Řezáč, C. G. Sánchez, M. Sternberg, M. Stöhr, F. Stuckenberg, A. Tkatchenko, V. W. Yu, T. Frauenheim. DFTB+, a software package for efficient approximate density functional theory based atomistic simulations; Sponsor Org.: USDOE Office of Science (SC), Basic Energy Sciences (BES) (SC-22). Chemical Sciences, Geosciences & Biosciences Division; National Science Foundation (NSF); CAREER Award; UKRI Future Leaders Fellowship; Engineering and Physical Sciences Research Council (EPSRC). 2020.

- 63. J. Řezáč. Empirical Self-Consistent Correction for the Description of Hydrogen Bonds in DFTB3. *J. Chem. Theory Comput.* **2017**, *13*, 4804-4817.
- 64. M. Kubillus, T. Kubař, M. Gaus, J. Řezáč, M. Elstner. Parameterization of the DFTB3 Method for Br, Ca, Cl, F, I, K, and Na in Organic and Biological Systems. *J. Chem. Theory Comput.* **2015**, *11*, 332-342.
- 65. M. Gaus, A. Goez, M. Elstner, M. Parametrization and Benchmark of DFTB3 for Organic Molecules. *J. Chem. Theory Comp.* **2013**, *9*, 338-354.
- 66. M. Gaus, X. Lu, M. Elstner, Q. Cui. Parameterization of DFTB3/3OB for Sulfur and Phosphorus for Chemical and Biological Applications. *J. Chem. Theory Comp.* **2014**, *10*, 1518-1537.
- 67. J. Řezáč, P. Hobza. Advanced Corrections of Hydrogen Bonding and Dispersion for Semiempirical Quantum Mechanical Methods. *J. Chem. Theory Comp.* **2012**, *8*, 141-151.
- 68. L. Martínez, R. Andrade, E. Birgin, J. M. Martínez. PACKMOL: A package for building initial configurations for molecular dynamics simulations. *J. Comp. Chem.* **2009**, *30*, 2157-2164.
- 69. F. Carey, R. Giuliano, N. Allison, B. Bane. Organic Chemistry; McGraw Hill: 2020.
- 70. S. J. Gumbley, R. Stewart. Effect of substituents at the 5-position on the first and second dissociation constants of isophthalic acid. *J. Chem. Soc.*, *Perkin Trans.* 2 **1984**, 529-531.
- 71. J. Towns, T. Cockerill, M. Dahan, I. Foster, K. Gaither, A. Grimshaw, V. Hazlewood, S. Lathrop, D. Lifka, G. D. Peterson, R. Roskies, J. R. Scott, N. Wilkins-Diehr. XSEDE: Accelerating Scientific Discovery. *Computing in Science & Engineering* **2014**, *16*, 62-74.